

Segmentation and Analysis of the Glomerular Basement Membrane in Renal Biopsy Samples Using Active Contours: A Pilot Study

Rangaraj M. Rangayyan,¹ Ilya Kamenetsky,¹ and Hallgrimur Benediktsson²

Some renal diseases cause changes in the structure of the glomerular basement membranes (GBM). Measurement of the thickness of the GBM can be performed on transmission electron microscopy (TEM) images of renal biopsy samples. Increased thickness of the GBM is observed in patients with diabetic nephropathy. Abnormally thin GBMs are associated with hematuria. We propose image processing methods for the detection and measurement of the GBM. The methods include edge detection, morphological image processing, active contour modeling, skeletonization, and statistical analysis of the width of the GBM. In the present pilot study, the methods were tested with 34 TEM images of six patients. The estimated mean and standard deviation of the GBM width for a patient with normal GBM were 348 ± 135 nm; those for a patient with thin GBMs due to hematuria were 227 ± 94 nm; and those for a patient with diabetic nephropathy were $1,152 \pm 411$ nm. Comparison with manual measurements by an experienced renal pathologist indicated low error in the range of 36 ± 11 nm.

KEY WORDS: Glomerular basement membrane, active contours, skeletonization, segmentation

INTRODUCTION

The Glomerular Basement Membrane and its Function in the Kidneys

The kidneys are responsible for the excretion of the body's waste products and maintenance of proper balance of water and electrolytes in the blood. Each kidney has an outer part called the cortex and an inner part called the medulla. The cortex contains filtration units, comprising the glomeruli and tubules. The medulla is made up of renal pyramids that collect the urine produced by the filtration units in the cortex.^{1,2} The main function of the glomerulus is to permit the passage of selected blood components through the filtration barrier; the ultrafiltrate is forced through the

Bowman's capsule and then drained out into the proximal convoluted tubule. The filtering action inside the glomerulus is achieved in two ways: by mechanical filtering of molecules larger than albumin (3.6 nm), and by preventing negatively charged molecules, such as plasma proteins, from passing through the barrier.³ Three types of structures participate in the filtering action: endothelial cells, the glomerular basement membrane (GBM), and the visceral epithelium (podocytes). The GBM plays a crucial role in both structural support and functional operation of the glomerulus. The typical width of the GBM in adults is normally in the range of 300 to 350 nm.^{1,2}

Imaging of Renal Biopsy Samples and Analysis of the GBM

Quantitative ultrastructural analysis of the GBM is an essential part of the examination of renal biopsies in many diseases, including essential hematuria,⁴ Alport syndrome (AS),^{5,6} thin-basement-membrane nephropathy (TBMN)^{7,8}, and diabetes

¹From the Department of Electrical and Computer Engineering, Schulich School of Engineering, University of Calgary, Calgary, AB, Canada T2N 1N4.

²From the Department of Pathology and Laboratory Medicine, University of Calgary, Calgary, AB, Canada T2N 1N4.

This paper submitted to the *Journal of Digital Imaging*, November 2008; revised January 2009.

Correspondence to: Rangaraj M. Rangayyan, Department of Electrical and Computer Engineering, Schulich School of Engineering, University of Calgary, Calgary, AB, Canada T2N 1N4; tel: +1-403-2206745; e-mail: ranga@ucalgary.ca

Copyright © 2009 by Society for Imaging Informatics in Medicine

Online publication 19 February 2009

doi: 10.1007/s10278-009-9188-6

mellitus.^{9,10} The primary method for the detection of AS relies on analysis of the GBM based on transmission electron microscopy (TEM) of biopsy samples of renal tissue from the patient. The typical lesion is characterized by a thickening of the GBM to the range of 800 to 1200 nm, with splitting and fragmentation of the lamina densa. In some patients, thickening of the GBM may be alternated with thinning of some portions of the GBM to the range of 100 to 200 nm. GBM thickness of less than 250 nm is used as a criterion for the diagnosis of TBMN.^{2,7,8} Diabetic nephropathy is a complex disorder with involvement of all tissue compartments of the kidney. An early change is a diffuse thickening of the GBMs. The pathogenesis of this alteration is poorly understood; it correlates with proteinuria and may be related to abnormal podocyte function.^{11,3}

Although morphometric analysis of the GBM is of importance to a pathologist, only a limited number of reliable techniques have been developed. Most of the methods for the measurement of GBM thickness are manual and rely on the techniques developed by Osawa et al.,¹² which define GBM width as the distance between the cytoplasmic membranes of the endothelium and the epithelial foot processes. Other popular methods rely on a sampling grid superimposed on the micrograph.^{7,8} Although some of the methods can be successfully applied on a limited dataset, the general use of the manual techniques is time-consuming and prone to interobserver variation. Only a few methods^{13,14} have been proposed with a limited degree of success in attempts to automate the detection and analysis of the GBM.

In the present paper, we propose methods for semiautomatic and user-guided methods for objective, reliable, and quantitative analysis of the GBM thickness in TEM images of renal biopsy samples. The methods include steps for edge detection,¹⁵ morphological image processing,¹⁶ active contour models (ACM),^{17,18} skeletonization,¹⁹ and statistical analysis of the width of the GBM.²⁰

METHODS

Image Acquisition

TEM is extensively used in medical applications to reveal the ultrastructure of biological samples to

the order of a few nanometers.^{21,22} The images used in the present study were acquired using a Hitachi H-7000 TEM system with magnification in the range of 1,500 to 17,000, and were digitally captured by an H-7000 4.2MP (megapixel) charge-coupled device (CCD) camera. The computer used to process the images is a Dell Precision 360 workstation with the following technical characteristics: 3.20 GHz Pentium 4 processor, 2 MB of cache memory, and 2 GB of RAM. Figure 1a shows an example of a TEM image including parts of a GBM.

The dataset used includes a total of 34 TEM images of renal biopsy samples of six patients: one patient with abnormally thin GBM, one with abnormally variable GBM width, two with normal GBM, and two with abnormally thick GBM. Some of the related details of the six patients are listed in Table 1. For each patient, one image was selected for manual segmentation and analysis, with several regions of interest (ROIs) comprising sections of the GBM. The images were processed independently by an experienced renal pathologist (HB) and the proposed methods, including segmentation of the GBM, measurement of its width, and computation of the statistics for comparative analysis.

Segmentation of the GBM Using Active Contours

The method proposed in the present work for segmentation of the GBM includes the following procedures:

1. detect the edges in the given image using Canny's method;¹⁵
2. perform morphological smoothing with a disc structuring element of radius 5 pixels;
3. build walls at breaks in the edge map to prevent the ACM from leaking into adjacent regions;
4. initialize the ACM contour;
5. set ACM deformation parameters;
6. control the deformation of the ACM;
7. save the contour, if the results are satisfactory;
8. initialize and deform additional contours, if necessary;
9. perform analysis of the width of the GBM; and
10. add the result to the cumulative statistics for the current case or patient.

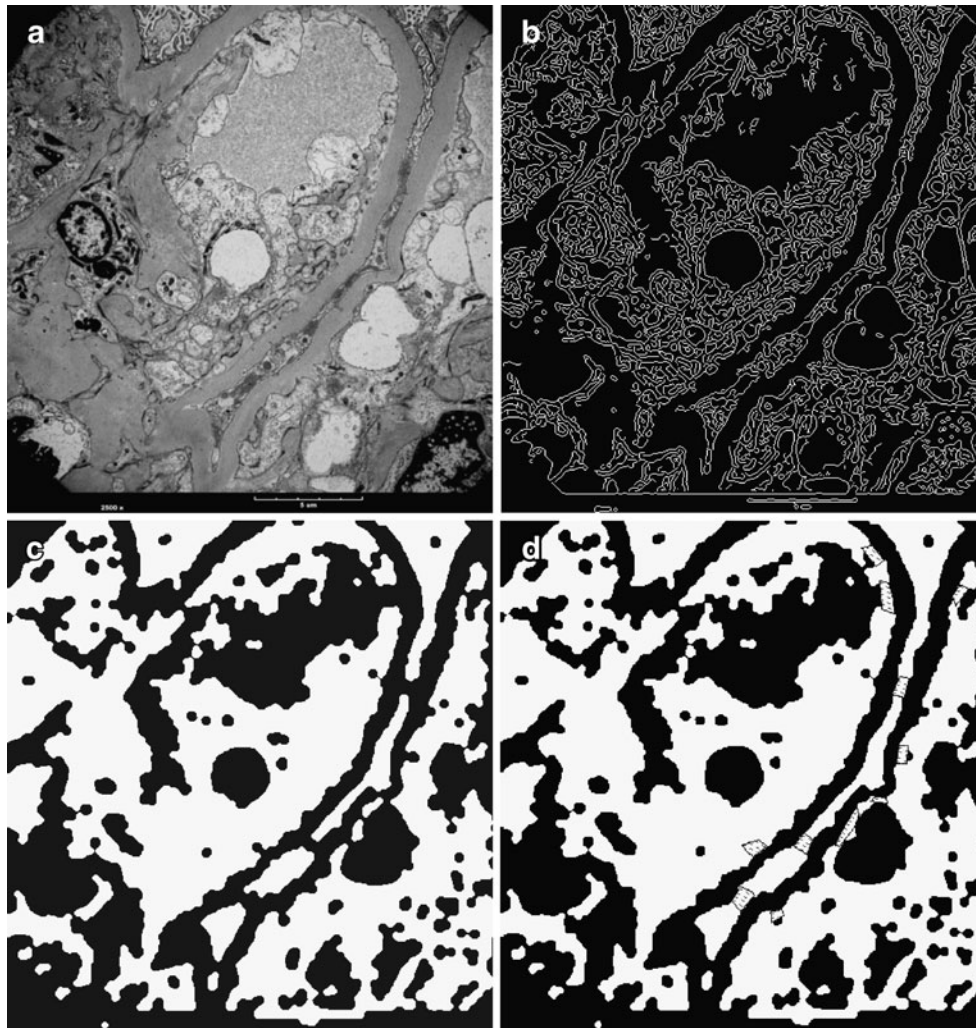


Fig 1. a A TEM image of a renal biopsy sample. The true length of the calibration bar in the image is 5 μm . Image size 485 \times 512 pixels, with a resolution of 21.4 pixels per micrometers. b The result of Canny edge detection. c Morphological smoothing of the image in (b) with a disc structuring element of radius 5 pixels. d Walls to block leakage of the ACM. The walls are shown as *hatched boxes* on the *black-and-white image*.

Table 1. Description of the Patients and TEM Images Used in the Present Work

Patient	Sex, age	Number of images	GBM distribution	Diagnosis
1	f, 60	6	Abnormally thin	Hematuria
2	f, 63	6	Abnormally variable	Hematuria and diabetes mellitus
3	f, 31	5	Normal	IgA nephropathy
4	f, 86	6	Normal	IgA nephropathy
5	m, 39	5	Abnormally thick	Diabetic nephropathy
6	m, 43	6	Abnormally thick	Diabetic nephropathy

Age is given in years

IgA immunoglobulin A, *f* female, *m* male

A single operator (IK) performed the analysis reported in the present work. Steps 3 and 4 in the procedure described above are manual; Steps 5–8 are semiautomatic. A graphical user interface (GUI) has been developed as part of the present work to facilitate the execution of the methods described above, as well as the subsequent steps described in the following paragraphs.

The ACM algorithm used in the present work is a modified version of an open-source code.²³ Because TEM images of renal biopsy samples comprise a variety of tissues with complex boundaries, the direct application of the ACM algorithm does not produce a satisfactory result. Instead, the ACM is applied to the morphological-

ly smoothed result of edge detection based on the Canny algorithm.

As can be seen from the result of edge detection in Figure 1b, the GBM is a smooth region without internal edges, whereas its external boundary is characterized by mostly continuous and strong edges. Because, at some locations, the boundary has gaps, which might permit leakage of the ACM during deformation, morphological smoothing¹⁶ is applied to the result of edge detection, leading to the result shown in Figure 1c.

The contour for ACM is initialized by the operator, and is then deformed under the influence of internal and external forces, until the minimum-energy equilibrium is reached. The internal forces

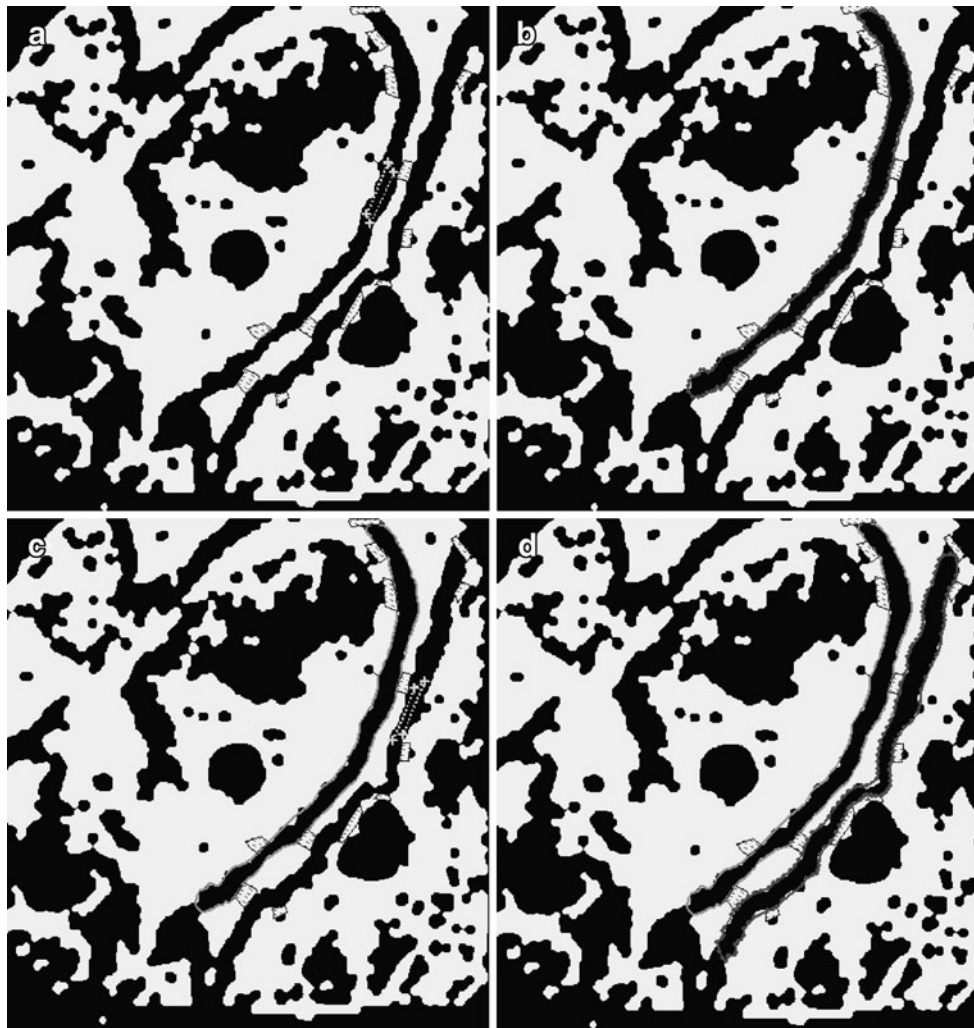


Fig 2. a First initial contour specified by the user for the image in Figure 1d. b The final stage of the first contour. c Second initial contour specified by the user for the same image. d The final stage of the second contour. The final contours in each case are shown in an intermediate shade of gray on the black-and-white image.

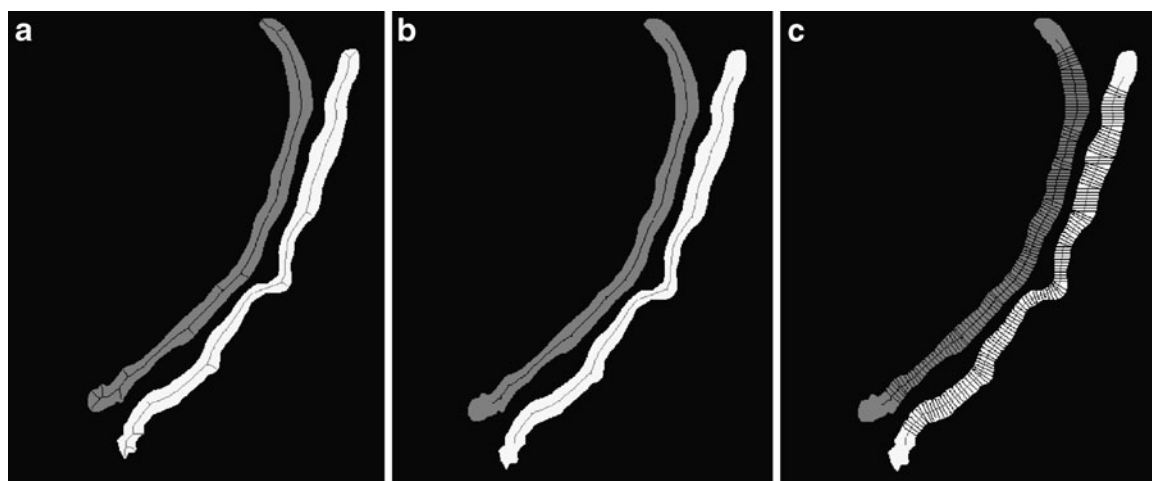


Fig 3. a Skeletons derived from the two segmented GBM regions shown in Figure 2d. b The skeletons after trimming of spurs. c Measurement of the GBM width in directions perpendicular to the skeleton of each contour. For the sake of clarity, the *measurement lines* are shown only for every third pixel.

are defined within the contour and are characterized by the contour's tension and rigidity. The traditional definition of the external force, based on the potential energy of the image, provides a good result when the initial contour is selected close to the object's boundaries. This, however, might not always be the case, particularly for objects having concavities in their boundaries. To address this limitation of the traditional potential force, several types of external forces^{17,18,24–26} have been proposed, with varying degrees of success. One of the successful methods, known as gradient vector flow (GVF), was proposed by Xu and Prince.²⁶ The GVF helps to diffuse the gradient of an edge map in regions distant from the boundary, substantially increasing the attraction range of the contour. The intensity of diffusion is set to be proportional to the strength of the object's edges, preventing undesirable distortion of the boundaries. The external force is the GVF, which is created by the diffusion of the gradient of the image's edge map. The parameters that influence the behavior of the ACM are modified from their default values by the operator using the GUI, if required.

At locations where the GBM is adjacent to other homogeneous regions, the boundary of the GBM may not be detected by Canny's procedure, or may be removed by morphological smoothing; this can cause leakage of the ACM contour to regions outside the GBM. To prevent this, the operator can construct a wall to restore the GBM boundary at

the desired location; see Figure 1d. Walls can also be used to prevent the leakage of one ACM contour into another, when multiple contours need to be constructed to cover the entire length of a GBM. Upon construction of the walls, the operator is guided to initialize the contour within a GBM area, to update the parameters and to start the deformation of the ACM. Figure 2a gives an example of the initialization of a contour; part (b) of the same figure shows the final result of the ACM for the initial contour provided. If the result of the deformation is acceptable, the user can save the contour, build walls at the ends of the contour, and continue with additional ACMs to cover the entire surface of the GBM within the image, as required. Figures 2c and d show the initialization and final result derived for a second ACM contour for the same image.

Table 2. Comparison of the Results Obtained with the Proposed ACM Method and Manual Measurements Performed by the Pathologist

Patient	Manual		ACM	
	μ	σ	μ	σ
1	164	60	191	50
2	393	106	358	77
3	205	42	171	29
4	442	118	417	141
5	1,173	213	1,227	248
6	1,109	237	1,152	390

μ and σ represent the mean and standard deviation of the GBM width in nanometers

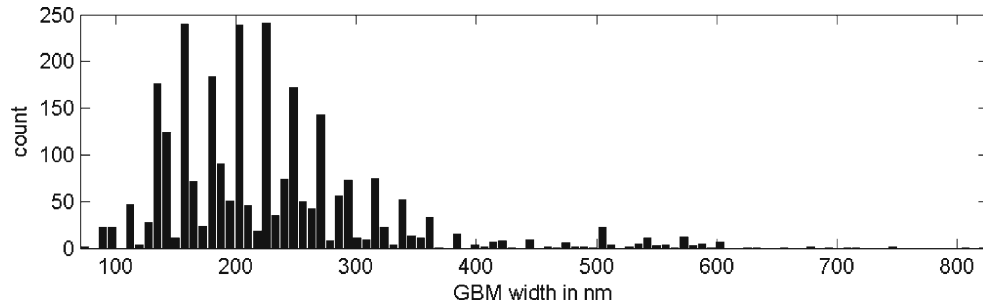


Fig 4. Cumulative histogram of the GBM width for the first patient using the ACM method with 16 ROIs from six TEM images.

Skeletonization of the GBM

After most of the GBM tissue present in the image being analyzed has been covered with multiple ACM contours, the results of segmentation are merged and passed on to a procedure for the detection of the skeleton. The skeleton is a binary, one-pixel wide representation of the given image that summarizes information related to the size, orientation, shape, and connectivity of the objects in the image.^{19,27} A point $h \in F$ belongs to the skeleton of F , if, for the largest disc centered at h , expressed as $D(h)$, there does not exist a disc D , such that $D(h) \subset D \subseteq F$.¹⁹ The skeletons of the GBM based on the two ACM contours shown in Figure 2d are displayed in Figure 3a.

In addition to pixels corresponding to the central line of the GBM, the skeletons obtained using the procedure described above were observed to contain several short segments due to the presence of protrusions, incursions, and minor details in the GBM [see Fig. 3a]. Such spurs or hair-like parts of the skeleton, if left intact, could lead to erroneous measurements of the GBM width, and therefore, have to be removed. The technique of “skeleton shaving”¹⁶ was applied for this purpose. When applied once, the procedure removes a single pixel

at each end of the skeleton. If the procedure is repeated N_s times, where N_s is called the “shaving depth,” such that N_s is larger than the length of the spurs, the remaining skeleton corresponds to the central line of the GBM. Figure 3b shows the result of “skeleton shaving” of the skeletons in Figure 3a, with a “shaving depth” $N_s=23$ pixels. It is seen that most of the spurs have been trimmed or removed.

The pixels of a given skeleton need to be linked together with the skeleton’s chains. The linking procedure starts at one of the skeleton’s ends and is carried on using the eight-connected neighborhood until the other end is detected. If, during the linking procedure, the skeleton splits into two or more branches, the linking for the current chain is terminated, and pixels corresponding to the beginnings of each branch are added to the list of the skeleton’s end-points, to form their own skeleton chains. Because a GBM image can comprise several disconnected regions, there can be many skeleton chains formed at the end of the linking procedure. The process ends when all skeleton points get linked to the skeleton chains. Upon completion of the linking procedure, the length of each skeleton chain is checked against the minimum length threshold. If a chain’s length is less

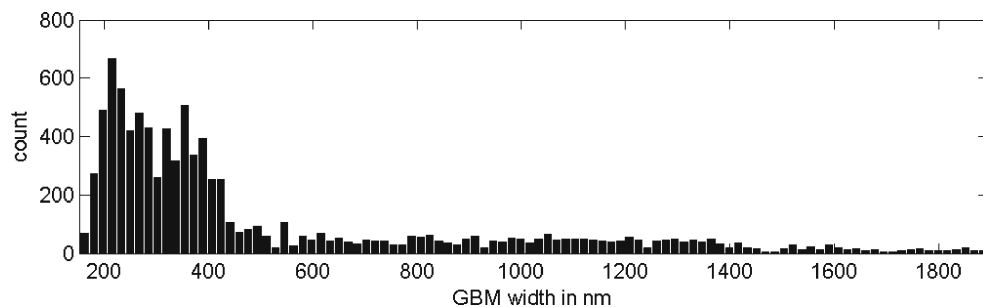


Fig 5. Cumulative histogram of the GBM width for the second patient using the ACM method with 14 ROIs from six TEM images.

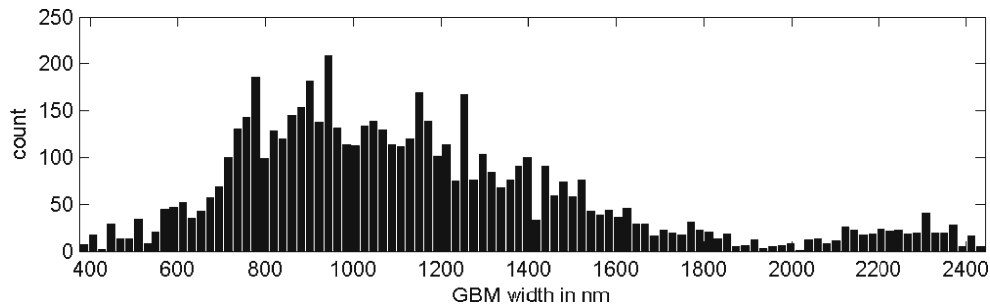


Fig 6. Cumulative histogram of the GBM width for the fifth patient using the ACM method with 11 ROIs from five TEM images.

than the specified minimum size (equal to 21 pixels in the present work), it is removed.

The values for the parameters shaving depth and minimum chain length need to be set taking into account the image resolution, magnification, the GBM width, the GBM length, the GBM shape, and the presence of protrusions and incursions. The values mentioned above were determined by experimentation and provided the best results for the set of images analyzed.

Measurement and Analysis of the Width of the GBM

The following procedure is then applied for the estimation of the GBM width:

1. Start with the first skeleton chain.
2. Denote by w the size of a sliding window and by l a chain's length. Place the sliding window at the beginning of the chain such that the first w elements of the chain are included in the analysis.
3. Fit a straight line to all the pixels within the sliding window and calculate its slope t .
4. Estimate the slope of the normal to the composed line as $n=-1/t$. If t is less than a

minimum slope threshold (equal to 0.2 in the present work), mark n as a vertical line.

5. Using the slope of the normal n and the pixel corresponding to the center of the sliding window, build the equation to the line perpendicular to the straight-line fit obtained in step 3.
6. Follow the perpendicular line in both directions from the skeleton pixel until the boundary of the GBM region is reached. If, during the growth procedure, the perpendicular line touches the image boundary or intersects with another skeleton point, discard the line.
7. Calculate the Euclidean distance between the two end points, corresponding to the intersections of the perpendicular line with the GBM boundary.
8. If the position of the sliding window is less than $l-w/2$, advance it by 1 to the next skeleton point and go to step 3; otherwise proceed to the next skeleton chain and go to step 2.

Figure 3c depicts the width measurements along the GBM using the skeletons of two contours resulting from ACM. The histogram of all of the GBM width measurements is accumulated for the case being processed, which could include several

Table 3. Cumulative Statistics of the GBM Width Distribution Obtained with the Proposed ACM Method

Patient	Number of Images	Number of ROIs	Statistics of GBM				With CV
			μ	σ	S	K	
1	6	16	227	94	2.0	8.6	0.4
2	6	14	512	387	1.5	5.4	0.8
3	5	11	357	215	1.1	3.6	0.6
4	6	17	348	135	0.9	3.8	0.4
5	5	11	1,152	411	1.1	4.0	0.4
6	6	17	1,111	383	0.7	3.2	0.3

The symbols μ , σ , S, K, and CV represent, respectively, the mean, standard deviation, skewness, kurtosis, and coefficient of variation. μ and σ are in nanometers

ROIs from several images. The following procedures are then applied for analysis of the GBM:

1. conversion of the width data from pixels to nanometers;
2. calculation of the mean (μ) and the standard deviation (σ);
3. rejection of the results at the extremes based on the distribution;
4. recalculation of μ and σ ;
5. estimation of skewness, kurtosis, and coefficient of variation ($CV=\sigma/\mu$);
6. plotting of the histogram of the GBM width measurements; and
7. updating the accumulated statistics.

The GUI developed as part of the present work facilitates the execution of the methods described above.

EXPERIMENTS AND RESULTS

The proposed methods were tested with 34 TEM images of six patients; see Table 1 and the “Image Acquisition” section for details. Compared with manual measurements performed on one image each of the six patients studied, the average and standard deviation of the differences in the mean widths provided by the ACM method were 36 ± 11 nm; see Table 2 for details.

The accumulated histograms for three of the six patients in the study are shown in Figures 4, 5, and 6. The statistics computed for all of the six patients in the study are shown in Table 3. The mean and standard deviation of the GBM width for one of the patients with normal GBM were estimated to be 348 ± 135 nm; those of a patient with thin GBMs associated with familial hematuria were 227 ± 94 nm; and those of a patient with thick GBM due to diabetes were $1,152\pm 411$ nm. For one of the patients with hematuria and diabetic nephropathy, demonstrating abnormally variable GBM width, the mean and standard deviation of the GBM width were 512 ± 387 nm, leading to the highest coefficient of variation observed of $CV=0.76$.

DISCUSSION AND CONCLUSION

The statistics of GBM width computed for the six patients in the study successfully demonstrate

the characteristic and expected distributions of the GBM width for each case, including abnormally thin, normal, abnormally variable, and abnormally thick GBM width. The present study demonstrates the viability of a semiautomated procedure for the segmentation and analysis of the GBM using ACM. Additional work is required on the development of improved edge detection algorithms to minimize the manual steps of wall construction in the proposed procedure. Methods for the detection of edges by nonlinear diffusion equations²⁸ and multiresolution contour detection by surround inhibition²⁹ could be explored for this purpose.

Further detailed analysis of the statistical distribution and parameters of the GBM, such as skewness and kurtosis, requires results from a larger database of images and cases. The present work represents a pilot study with a small set of cases and images. Further work is planned with a larger database of clinically proven cases. The proposed methods should reduce the effort required to analyze TEM images of renal biopsy samples, and lead to improved quantitative analysis of the GBM.

REFERENCES

1. Vize PD, Woolf AS, Bard JBL: *The Kidney, From Normal Development to Congenital Disease*. London, UK: Academic, 2003
2. Schwartz MM, Jennette JH, Olson JL, Silva FG: *Pathology of the Kidney*, 6th edition. New York, NY: Lippincott Williams & Wilkins, 2007
3. Moriya T, Groppoli TJ, Kim Y, Mauer M: Quantitative immunoelectron microscopy of type VI collagen in glomeruli in type I diabetic patients. *Kidney Int* 59:317–323, 2001
4. Coleman M, David W, Haynes G: Glomerular basement membrane abnormalities associated with apparently idiopathic hematuria. *Human Pathol* 17:1022–1030, 1986
5. Gubler MC, Levy M, Broyer M: Alport's syndrome: a report of 58 cases and a review of the literature. *Am J Med Sci* 70:493–505, 1981
6. Habib R, Gubler MC, Hinglais N: Alport's syndrome: experience at Hospital Necker. *Kidney Int* 11:20–28, 1982
7. Saxena S, Davies DJ, Kirsner RLG: Thin basement membranes in minimally abnormal glomeruli. *Prog Clin Pathol* 43:32–38, 1990
8. Basta-Jovanovic G, Venkataseshan VS, Gil J: Morphometric analysis of glomerular basement membranes in thin basement disease. *Clin Nephrol* 33:110–114, 1990
9. Osterby R: Thin glomerular basement membrane nephropathy: incidence in 3471 consecutive renal biopsies examined by electron microscopy. *Arch Pathol Lab Med* 130:699–706, 2006
10. Osterby R: Morphometric studies of the peripheral glomerular basement membrane in early juvenile diabetes. I.

Development of initial basement membrane thickening. *Diabetologica* 8:84–92, 1972

11. Li JJ, Kwak SJ, Jung DS, Kim JJ, Yoo TH, Ryu DR, Han SH, Choi HY, Lee JE, Moon SJ, Kim DK, Han DS, Kang SW: Podocyte biology in diabetic nephropathy. *Kidney Inter Suppl S*:36–42, 2007
12. Osawa G, Kimmelstiel P, Sailing V: Thickness of glomerular basement membranes. *Clinical Pathology*, 45:7–20, 1966
13. Ong SH, Giam ST, Jayasooriah, Sinniah R: Adaptive window-based tracking for the detection of membrane structures in kidney electron micrographs. *Mach Vis Appl* 6:215–223, 1993
14. Ong SH, Jin XC, Jayasooriah, Sinniah R: Image analysis of tissue sections. *Comput Biol Med* 26:269–279, 1996
15. Canny J: A computational approach to edge detection. *IEEE Trans Pattern Anal Mach Intell* 8(6):679–698, 1986
16. Goutsias J, Batman S: Morphological methods for biomedical image analysis. In: Sonka M, Fitzpatrick JM Eds. *Handbook of Medical Imaging, Volume 2: Medical Image Processing and Analysis*. Bellingham, WA: SPIE, 2000, pp 175–272
17. Kass M, Witkin A, Terzopoulos D: Snakes: Active contour models. *Int J Comput Vis* 1:321–331, 1987
18. Xu C, Pham DL, Prince JL: Image segmentation using deformable models. In: Sonka M, Fitzpatrick JM Eds. *Handbook of Medical Imaging, Volume 2: Medical Image Processing and Analysis*. Bellingham, WA: SPIE, 2000, pp 129–174
19. Gonzalez RC, Woods RE: *Digital Image Processing*. Reading, MA: Addison-Wesley, 1993
20. Rangayyan RM, Kamenetsky I, Benediktsson H: Segmentation and analysis of the glomerular basement membrane

using active contour models. In *The IET 4th International Conference on Advances in Medical and Signal Processing (MEDSIP 2008)*, page Paper 2.1.3 (4 pages), Santa Margherita Ligure, Italy, July 2008

21. Rangayyan RM: *Biomedical Image Analysis*. Boca Raton, FL: CRC, 2005
22. Wgrowska-Danilewicz M, Danilewicz M: Current position of electron microscopy in the diagnosis of glomerular diseases. *Pol J Pathol* 58:87–92, 2007
23. Hamarneh G: The Active Contour Model Matlab open source code. <http://www.cs.sfu.ca/~hamarneh/software/acm/index.html>, School of Computing Science, Faculty of Applied Science, Simon Fraser University, Vancouver, BC, Canada, 2007
24. Cohen LD: On active contour models and balloons. *Comput Vis Graph Image Process* 53:211–218, 1991
25. Cohen LD, Cohen I: Finite-element methods for active contour models and balloons for 2-d and 3-d images. *IEEE Trans Pattern Anal Mach Intell* 15:1131–1147, 1993
26. Xu C, Prince JL: Snakes, shapes, and gradient vector flow. *IEEE Trans Image Process* 7:359–369, 1998
27. Blum H: A transformation for extracting new descriptors of shape. In: Wathen-Dunn W Ed. *Models for the Perception of Speech and Visual Form*. Cambridge, MA: MIT, 1967
28. Perona P, Malik J: Scale-space and edge detection using anisotropic diffusion. *IEEE Trans on Pattern Anal Mach Intell* 12(7):629–639, 1990
29. Papari G, Campisi P, Petkov N, Neri A: Contour detection by multiresolution surround inhibition. In *IEEE International Conference on Image Processing*, pages 749–752. IEEE, 2006